Journal of Molecular Structure 1225 (2021) 129176

Contents lists available at ScienceDirect

Journal of Molecular Structure

journal homepage: www.elsevier.com/locate/molstr

Costus speciosus koen leaf extract assisted cs-znx ($X = O$ or S) nanomaterials: Synthesis, characterization and photocatalytic degradation of rr 120 dye under uv and direct sunlight

S. Ravikumar[a], V. Pandiyan[a,*], Manawwer Alam[c], Naushad Ahmad[c], V. Nithya[d], Balu Krishnakumar[b,*], Abilio J.F.N. Sobral[b]

[a] Department of Physics, Nehru Memorial College (Autonomous), Puthanampatti- 621 007, Tamil Nadu, India
[b] Chemistry Department, University of Coimbra, 3004-535 Coimbra, Portugal
[c] Department of Chemistry, College of Science, Riyadh-11451, King Saud University, Riyadh, Kingdom of Saudi Arabia
[d] Department of Animal Health and Management, Pharmacognosy Lab, Alagappa University, Karaikudi-630 003, Tamil Nadu, India

ARTICLE INFO

Article history:
Received 21 June 2020
Revised 28 August 2020
Accepted 29 August 2020

Keywords:
Reactive red 120
CS-ZnO
CS-ZnS *costus speciosus koen*
Photocatalytic activity

ABSTRACT

The distinct nanocrystalline CS-ZnX ($X = O$ or S) were achieved through *Costus speciosus* Koen leaf extract assisted precipitation cum hydrothermal method. The formation of the materials was confirmed by different characterization techniques such as XRD, FT-IR, Raman, FE-SEM, EDS, HR-TEM, DRS, and PL measurements. The photocatalytic activity of the prepared materials was tested on the decolourization of Reactive Red 120 dye (RR 120) aqueous solution. The photocatalytic activity was further confirmed by Acid Black 1 (AB 1) dye degradation. The dye photocatalytic process was investigated by considering the influence of test parameters such as catalyst concentration and initial dye pH. Moreover, complete decolourization of 50 ppm of RR 120 solution was achieved within 180 min at pH 5. Both catalysts were found to be reusable. The photocatalytic degradation of RR 120 by CS-ZnX ($X = O$ or S) were confirmed GC–MS analysis, and suitable degradation pathways were proposed based on molecular ion and fragmentation peak values. The probable degradation mechanism was proposed and discussed.

1. Introduction

Organic dyes are used in industry, such as textiles, paper, paint, and bio-medical are non-biodegradable because of its complex chemical structure. These dyes have produced adverse effects and several uncurable problems for the environment and human health [1]. Many researchers in these fields are hardly working to find a suitable solution for this problem using nanotechnology but no suitable results have been obtained so far. Recently, zinc oxide and zinc sulfide (ZnS) are proved to be a favourable nanomaterial for different applications such as nano-sized sensors [2], photodiode, and photocatalyst [3-5] for the degradation of organic dyes [6,7]. It has been acting as a semiconductor material with a high bandgap energy of ZnO (3.37 eV) and ZnS (3.72 eV) [8,9]. Moreover, these photocatalysts produce hydroxyl radicals via charged holes (h^+) and excited electrons (e^-) which are the main reactive species for oxidative/reductive degradation of a wide range of organic pollutants. Generally, it has been found that these materials are more active in the UV region than solar for the degradation of various harmful organic dyes [10]. Nowadays the well-known biological strategy for the synthesis of NPs using microorganisms is a versatile method to solve the environmental-related problems in various streams [11-13]. Enzymes and plants or plant leaf extracts are recommended as chemical and eco-friendly alternatives to chemical and physical methods. The efficiency of NP for degradation of dyes obtained from this rout has proved to be the best due to its performance against pollutants. There are numerous works found in the literature stating that it has been a new simple and environmental benefit of green synthesis processes. Those are used for toxic chemicals and high energy input avoided. Recently, different types of research work have been undertaken to determine the bio-reduction of various metal ions and metal NPs [14-16].

Costus speciosus is one of a medicinal plant belonging to the family of Costaceae. Its common names are crepe ginger, canereed, malay ginger, spiral flag, and wild ginger. *Costus speciosus* has been traditionally used in Ayurveda to treat fever, rash, asthma, rancidity, and intestinal worms. In our earlier work, *Costus speciosus* leaf extract was used for the preparation of silver (CS-Ag) and

* Corresponding authors.
E-mail addresses: pandiyanphy@gmail.com (V. Pandiyan), chemkrishna2006@yahoo.co.in (B. Krishnakumar).

https://doi.org/10.1016/j.molstruc.2020.129176
0022-2860/

platinum (CS-Pt) nanoparticles and followed by the solvothermal synthesis of TiO_2 based nanocomposites [17,18]. In the present study, *Costus speciosus* leaf extract was used for the solvothermal synthesis of ZnX ($X = O$ or S) nanomaterials, *Costus speciosus* leaf extract was used as a capping agent rather than as a reducing agent. Characterization studies show that the prepared materials have crystallinity and uniformity and also were used as photocatalyst for degradation of the dye Reactive Red 120 under UV and solar light. The photocatalytic reusability of the photocatalyst was tested up to a four-time successive cycle and the particles still retain their high activity of photodegradation ratio. The degradation pathway has also been proposed for the degradation of RR 120 by CS-ZnO and CS-ZnS using GC–MS analysis.

2. Materials and methods

2.1. Chemicals

Zinc acetate dihydrate, thioacetamide, NaOH, RR 120 (CAS No: 61,951–82–4, molecular weight- 1496.98 g/mol, molecular formula ($C_{44}H_{24}Cl_2N_{14}Na_6O_{20}S_6$), Acid Black 1 (AB 1) dye and other chemicals used in this study were obtained from Aldrich and used as received. Plant materials (*Costus speciosus* Koen) were collected from Jawaharlal Nehru Tropical Botanical Garden and Research Institute (JNTBGRI), Trivandrum, India. Leaf extract was prepared according to our previous report [17,18].

2.2. Synthesis of CS-ZnO and CS-ZnS

Precipitation cum hydrothermal method was adopted for the synthesis of CS-ZnX ($X = O$ or S) materials. About 0.04 M of (8.76 g) of zinc acetate dihydrate was dissolved in 40 mL of water followed by addition of 5 mL of *Costus speciosus* Koen leaf extract; this was stirred for 20 to 30 min. To this, 40 mL water containing 0.16 M of (6.4 g) NaOH was added, and the stirring was continued for 3 h. The gel obtained was transferred into a 100 mL Teflon lined stainless-steel autoclave. The autoclave was maintained at 140 °C for 15–20 h and subsequently, cooled to room temperature. The precipitate was filtered washed with water and ethanol and dried at 80 °C for 5 h, the obtained CS-ZnO was stored for further use. For CS-ZnS, instead of NaOH, 0.04 M (3.004 g) of thioacetamide was used.

2.3. Characterization

The crystal structure of CS-ZnO and CS-ZnS nanoparticles has been studied by Powder X-ray diffraction (PXRD) patterns using a PANalytical X'Pert PRO powder X-ray Diffractometer with 15KVA UPS support at 2θ range of 10–80°. The optical properties of the sample were analyzed by UV–Vis Diffuse Reflectance Spectroscopy (UV-DRS) with Thermo Fisher Evaluation 220 in the range of 190–1100 nm range. Raman spectra were measured with a micro Raman Spectrometer, imaging spectrograph STR 500 mm Focal Length Laser Raman spectrometer with flat field: 27 mm(W) × 14 mm (H) and resolution: 1/0.6 cm^{-1}/pixel. Photoluminescence (PL) spectra were recorded using a Varian Cary Eclipse Photoluminescence spectrophotometer with oxford low-temperature LN2 77 K set up. The morphologies of the obtained products were observed by field emission scanning electron microscope (FE-SEM) observation was carried out on a BRUKER FE-SEM instrument along with an energy dispersive X-ray spectrum (EDS) as well as with high-resolution transmission electron microscope (HR-TEM) (FEI –TECNAI G2–20 TWIN with LaB6 filaments) operated at an accelerating voltage of 200 kV). The absorption spectra were recorded using a Perkin-Elmer UV spectrometer lambda 35. The solution of pH values was adjusted H_2SO_4 or NaOH using a (Systronics) Digital pH meter.

2.4. Photocatalytic methodology

The photocatalytic degradations of Reactive Red 120 (50 ppm) aqueous solution in the liquid phase were conducted in a glass tube with 2.5 cm inner diameter and 37 cm length. Four 8 W mercury UV lamps with a wavelength centered at 365 nm were used as the irradiation. Furthermore, the reactions were carried out under solar irradiation. A photocatalyst (50 mg) was suspended in 100 mL of (RR 120) dye solution and establishment of adsorption-desorption equilibrium measured for stirred at 30 min. An aliquot (3 mL) was taken at a certain time interval during the experiment and centrifuged (REMI-R- 8C) used to remove the powders. The filtered was analyzed on a Perkin-Elmer UV–vis spectrometer. The photocatalytic degradation of Acid Black 1 (AB 1) was carried out in an immersion type photoreactor (Heber immersion type photoreactor model HP-SLJV16254) [19]. A photocatalyst (50 mg) was suspended in 100 mL of 10 ppm of AB 1 dye solution.

2.5. GC–MS analysis

The intermediate product identifications were performed employing a gas chromatography-mass spectrometer (GC–MS) system. The GCMS (Shimadzu QP2020-NX, Columbia, Maryland, United States) is equipped with a direct connection with the capillary column. GC column was operated in temperature-programmed mode with 50 to 350 °C. The injection port temperature maximum of 450 °C with Helium served as the carrier gas column flow rate 15 mL/min. The sample for (GC–MS) analysis was prepared by extraction of a part of 50 mL of the irradiated solution (after the removal of CS-ZnO particles) with extraction repeated three times with 50 mL of dichloromethane each time. The organic layer (dichloromethane) was collected in a beaker. Some amount of anhydrous sodium sulfate (to remove H_2O) has been added, filtered and evaporate in air. After evaporation, just add an HPLC grade methanol (1 or 2 mL) in the beaker and shake well, and then subjected to GC–MS analysis. The same procedure adopted for the CS-ZnS sample.

3. Results and discussion

3.1. Characterization of the prepared materials

3.1.1. XRD spectra

In order to understand the phase analysis of the synthesized photocatalyst, XRD technique has been used is depicted in a Fig. 1. It has been found that the peaks at 31.67°, 34.31°, 36.14°, 47.40°, 56.52°, 62.73°, 66.28°, 67.91°, 69.03°, 72.48°, and 77.43° were assigned to the following planes *viz.* (100), (002), (101), (102), (110), (103), (200), (112), (201), (004), and (202) these are compared with the diffraction peaks from the standard card (JCPDS NO. 80–0074) and confirmed with the presence of a wurtzite structure in CS-ZnO (Fig. 1a). Fig 1b represents the X-ray diffraction patterns of CS- ZnS, it shows the obtained peaks are 29.31°, 34.1°, 47.93°, 57.30°, 69.9°, and 77.2° belongs to the diffraction planes of (111), (220), (100), (311), (400), and (331) resulting in the cubic zinc blende structure, which matched well with the standard card (JCPDS NO. 05–0566).

3.1.2. FT-IR spectra

FT-IR spectroscopy is used to identify the functional group present in the materials. The presence of expected functional groups along with their chemical bonds in a prepared composite are studied in the range of (400 - 4000 cm^{-1}) at room temperature. The FT-IR spectra of CS-ZnO and CS-ZnS are depicted in Fig. 2.

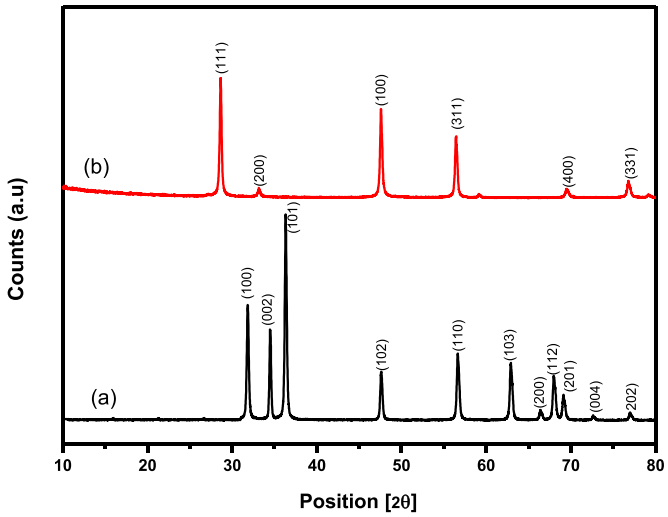

Fig. 1. XRD patterns of (a) CS-ZnO and (b) CS-ZnS.

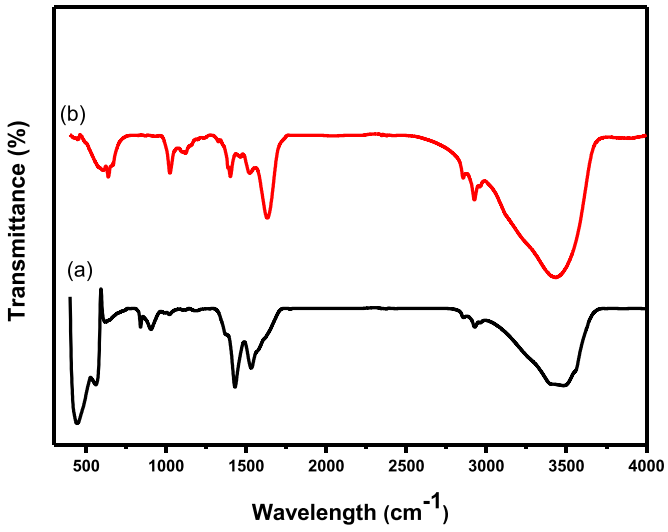

Fig. 2. FT-IR spectra of (a) CS-ZnO and (b) CS-ZnS.

In Fig. 2a, the absorption peak between 3356 and 3700 cm^{-1} corresponds to the O–H stretching of surface water molecule adsorbed on the surface of photocatalysts. The C–H absorption peaks have been observed between 2890 and 2950 cm^{-1}. The two bands occurring in the region of 1440–1620 cm^{-1} and correspond to the different modes of CO_3^{2-} (Fig. 2). All this information indicates the presence of zinc acetate precursors or maybe from *Costus species* leaf extract. The peak of the nanosized ZnO is observed in the range between 480 and 490 cm^{-1} in CS-ZnO (Fig. 2a). In Fig. 2b, it is obvious that the FT-IR spectra of ZnS particle show wide band between 3300 and 3600 cm^{-1} corresponds to the stretching vibration of O–H, which indicates the presence of adsorbed water molecules on the surface of photocatalyst. The characteristic ZnS vibration peaks can be noticed around the bands of 890 cm^{-1} and 689 cm^{-1} in the CS-ZnS sample [20] (Fig. 2b).

3.1.3. UV-DRS

The UV–Vis diffuse reflectance spectra (DRS) of the samples are shown in Fig. 3. It can be found that CS-ZnS has higher absorption than CS-ZnO in both UV (250–350 nm) and visible region (400 - 500 nm). In the UV region between 351 and 380 nm, CS-ZnO has higher absorption than CS-ZnS. The band gap energies of the prepared materials have been calculated using modified Kubelka-

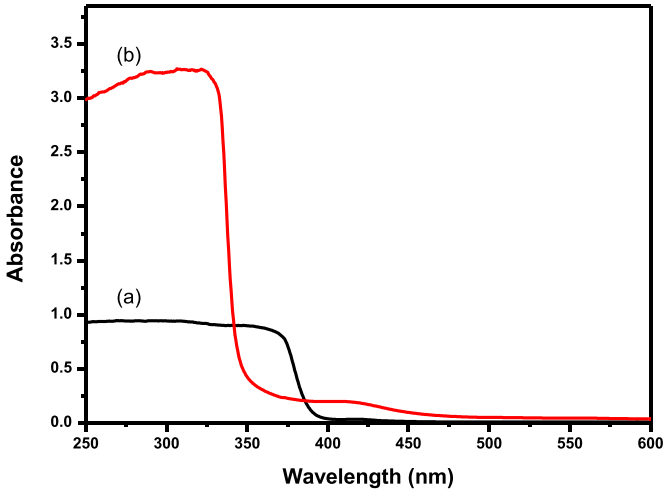

Fig. 3. DRS of (a) CS-ZnO and (b) CS-ZnS.

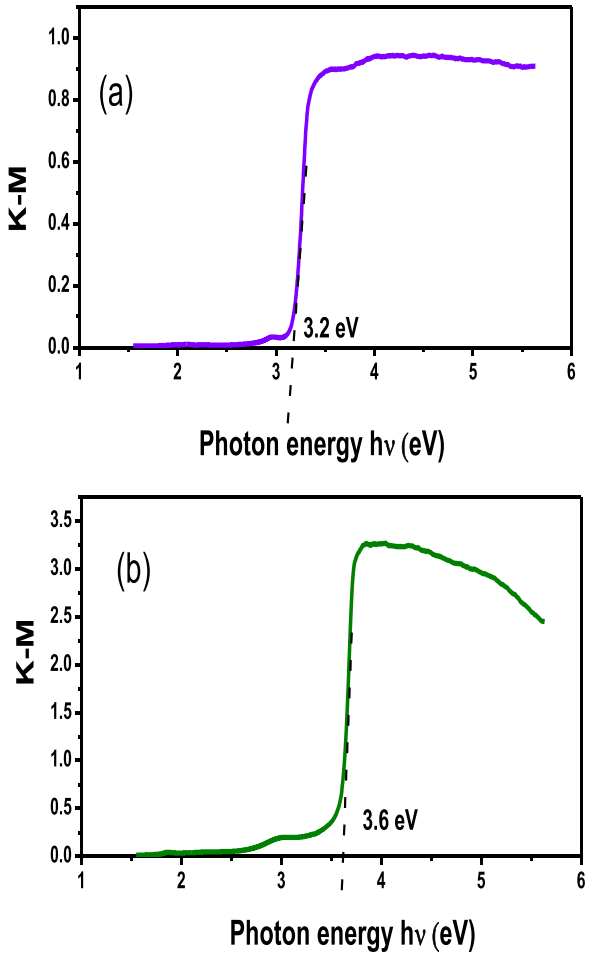

Fig. 4. KM plot of (a) CS-ZnO and (b) CS-ZnS.

Munk function (KM) was applied to find the band gap energies of the materials. The band gap energies of the CS-ZnO and CS-ZnS were found to be 3.2 and 3.6 eV, respectively (Fig. 4).

3.1.4. Raman spectra

Based on Raman selection rule, only E_2 and A1(LO) modes are allowed when the light propagation is parallel to the c-axis of the wurtzite structure. Fig. 5 shows that the Raman spectra of CS-ZnO

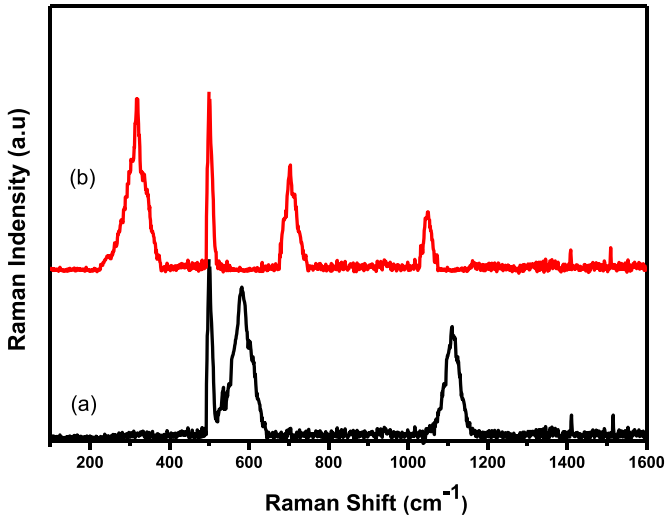

Fig. 5. Raman spectra of (a) CS-ZnO and (b) CS-ZnS.

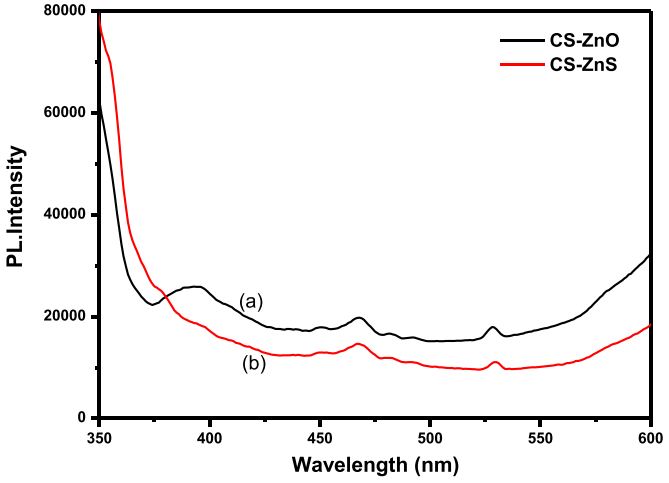

Fig. 6. PL spectra of (a) CS-ZnO and (b) CS-ZnS.

(Fig. 5a) and CS-ZnS (Fig. 5b). Although the E_2 mode peak between 400 and 450 cm^{-1} was not observed, while the peak around at 580 cm^{-1} is assigned to A_1 (lattice oxygen) mode of the hexagonal ZnO [21,22]. The Raman bands in the region from 1000 to 1400 cm^{-1} are attributed to the optical overtones and associated with the second-order Raman active modes of ZnO (Fig. 5a). In Fig. 5b, the Raman band at 330 cm^{-1} is assigned to E_1 (LO) mode of ZnS [23]. The peaks at 715 cm^{-1} and 1080 cm^{-1} can be found and indexed to longitudinal optical (LO) modes [24]. These peaks are in accordance with the characteristic Raman peaks of ZnS. Besides ZnS and ZnO, the Raman spectra of the samples show a new peak around 500 cm^{-1} in both samples may be due to *Costus speciosus* residue [17,18].

3.1.5. Photoluminescence spectra

The occurrence of photoluminescence intensity is due to electron–hole recombination, which is directly proportional to the rate of electron–hole recombination. CS-ZnO gave three emissions at 380 nm, 470 nm, and 530 nm (Fig. 6a). The emission spectrum of CS-ZnS nanoparticles show blue emission centered around 468 nm (Fig. 6b). This originates from the surface defect states such as sulfur vacancies located at the surface of ZnS nanoparticles [25]. The green emission peak observed at 533 nm can be attributed to the zinc vacancies [26].

3.1.6. FE-SEM and HR-TEM

The morphology of the prepared materials is analyzed by field emission scanning electron microscope (FE-SEM) analysis. FE-SEM images of CS-ZnO and CS-ZnS are shown in Fig. 7. For CS-ZnO, the particles are well separated and ellipse/cylinder shaped particles are seen (Fig. 7a&b). Some round-shaped particles are observed for CS-ZnS (Fig. 7c&d). The morphology of the prepared materials is further analyzed by high-resolution transmission electron microscope (HR-TEM) images. The HR-TEM images of the prepared materials are shown in Fig. 8. The ellipse/cylinder shaped particles of CS-ZnO is seen in Fig. 8a and Fig. 8b along with SEAD pattern and finger-print region (Fig. 8c and Fig. 8d). The length and width of the cylinder particles are 230 and 120 nm, respectively (Fig. 8b). The HR-TEM images (Fig. 8e and Fig. 8f) of CS-ZnS are shown along with SEAD pattern and finger print region (Fig. 8g and Fig. 8h) and reveals that some of the particles are round in shape. The diameter of the round-shaped particles is approximately 50–100 nm. The energy dispersive spectra of the CS-ZnO and CS-ZnS are shown in Fig. S1 and Fig. S2, respectively (see Supporting information's). The EDS analysis reveals that presence of Zn,O and Zn,S in CS-ZnO and CS-ZnS, respectively.

3.2. Photocatalytic study and effect of operational parameters

3.2.1. Photodegradation of RR 120 and AB 1 dyes

The photodegradation of RR 120 dye under UV and direct sunlight has been carried out with prepared catalysts and the results are displayed in Fig. 9. The dye RR 120 is resistant to self-photolysis. About 96% and 82% of decolourization observed when the dye is irradiated under UV light in the presence of CS-ZnS and CS-ZnO, respectively at 180 min irradiation. CS-ZnS is found to be efficient when compared with CS-ZnO in UV irradiation. The same experiment was performed with direct sunlight, about 80% and 59% of decolourization observed for CS-ZnS and CS-ZnO, respectively. As in UV, similar trend was observed with solar light. The overall, UV process was found to be more efficient when compared with the solar process. The order of activity is found to be CS-ZnS (UV)> CS-ZnO (UV) > CS-ZnS (solar) > CS-ZnO (solar). UV–Visible spectra of the dye (RR 120) at different times of irradiation are shown in Fig. 10. The absorbance between 400 and 800 nm corresponds to an $n \rightarrow \pi^*$ transition of the azo and hydrazone forms of the dye, which is due to the color of the azo dyes. The absorbance at 200–400 nm is attributed to the $\pi \rightarrow \pi^*$ transition of benzene rings, representing the aromatic content of azo dye. As the reaction time increased both in UV and solar processes, all of the peaks decreased gradually. No new peak appeared during irradiation in the analyzed wavelength range. This indicates that the dye molecule was destroyed in the presence of CS-ZnO and CS-ZnS under UV and solar irradiation. Furthermore, these spectra also reveal that intermediates do not absorb at analytical wavelengths.

The photocatalytic activities of the prepared materials are further tested with AB 1 dye degradation in an immersion type photoreactor under UV light irradiation and the results are shown in Fig. 11. When AB 1 solution was irradiated in the presence of CS-ZnS and CS-ZnO, about 90% (curve a) and 88% (curve b) of decolourization occurred ($\pi \rightarrow \pi^*$ transition- 615 nm), respectively at 90 min of irradiation. However, 85% (curve a) decolourization achieved within 45 min for CS-ZnS, at the same time only 57% (curve b) decolourization was achieved for CS-ZnO. Although within 45 min 85% (curve a) of decolourization achieved by CS-ZnS, and there was no significant increase in the activity observed after 45 min. CS-ZnS is found to be efficient when compared with CS-ZnO for decolourization of AB 1 dye. However, the trend is reverse for the degradation of the same dye. The degradation was monitored at 320 nm ($n \rightarrow \pi^*$ transition). About 79% (curve c) of degradation was achieved for CS-ZnO at 90 min of irradiation.

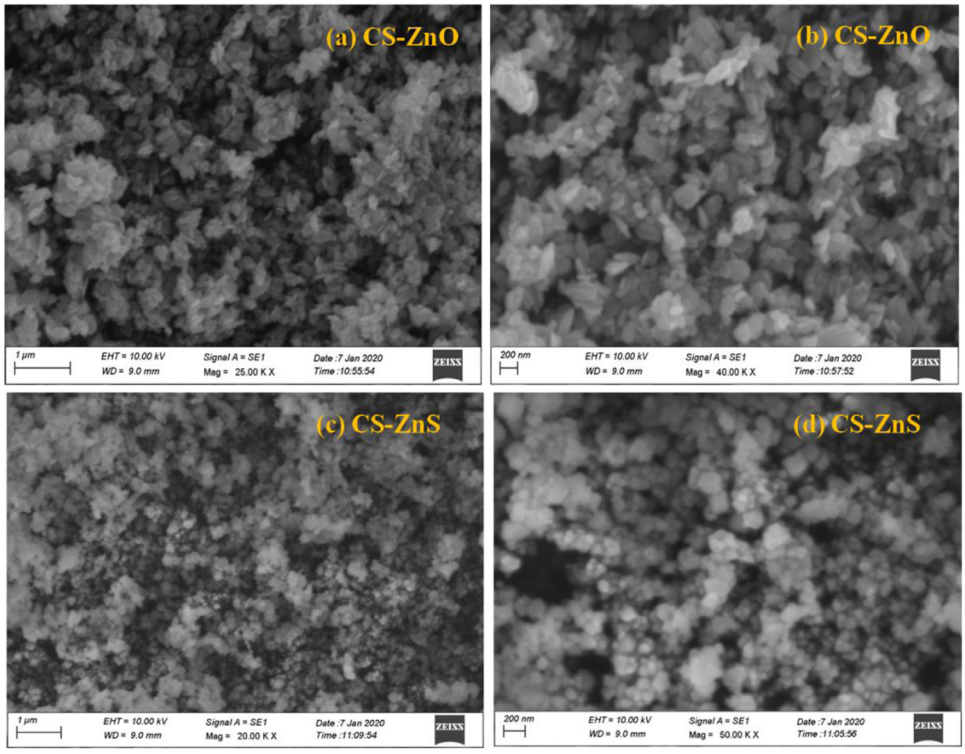

Fig. 7. FE-SEM images of (a&b) CS-ZnO and (b&c) CS-ZnS.

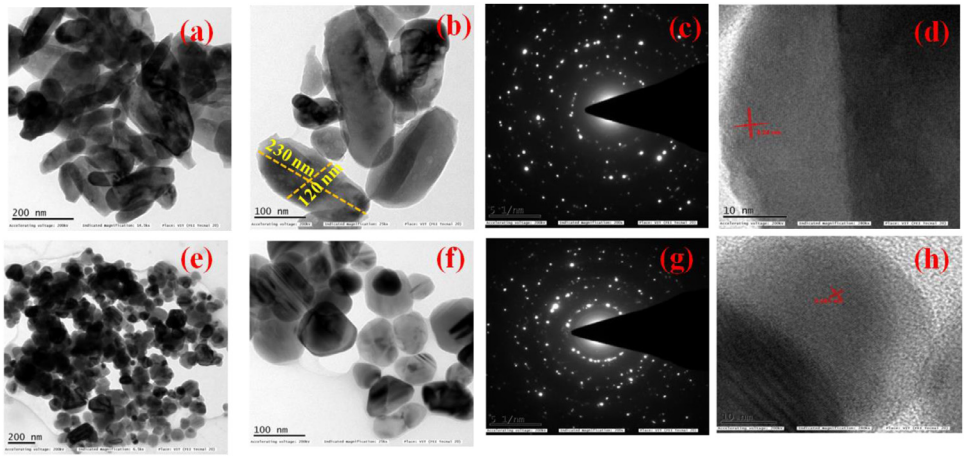

Fig. 8. HR-TEM images of (a and b), SEAD pattern (c), fingerprint region (d) of CS-ZnO and HR-TEM images of (e and f), SEAD pattern (g), fingerprint region (h) of CS-ZnS.

At the same condition, only 41% (curve d) of degradation was achieved for CS-ZnS. Here also, there was no significant increase in the degradation observed for CS-ZnS after 45 min of irradiation. For the degradation of AB 1, CS-ZnO is found to be efficient when compared with CS-ZnS. Overall, the order of activity is found to be CS-ZnS (decolourization) > CS-ZnO (decolourization) > CS-ZnO (degradation) > CS-ZnS (degradation). UV–Visible spectra of the dye (AB 1) at different times of irradiation along with its structure are shown in Fig. S3. Since almost complete decolourization of RR 120 dye observed under the UV process, the effect of operational parameters was carried out for this process.

3.2.2. Effect of initial dye pH

The pH is one of the important parameters which influence the photocatalytic activity. Therefore, it is better to study the effect of pH on photodegradation of RR 120 dye. Effect of initial pH on photodecolourization of RR 120 dye under UV and solar light with CS-ZnO and CS-ZnS have been investigated and the results are shown in Fig. 12. The decolourization of RR 120 is slightly influenced by pH in both processes. When pH increases from 3 to 5 for CS-ZnO/solar and CS-ZnS/solar processes, the percentage of decolourization increases from 53 to 59 and 70 to 80, respectively. The same trend was observed for UV process, the percentage of

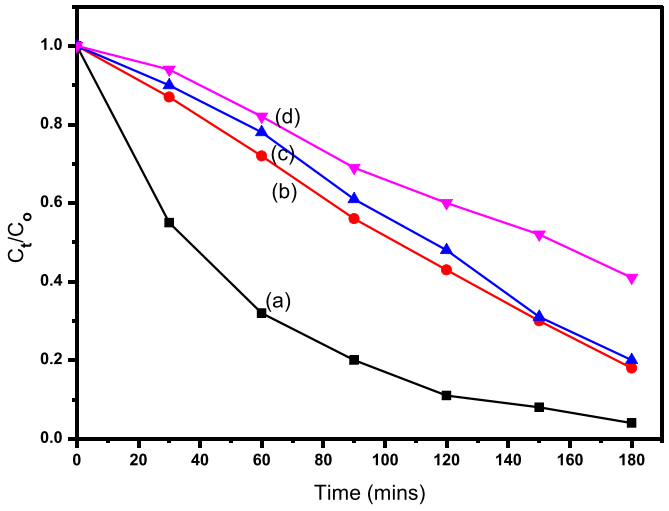

Fig. 9. Photodegradability of RR 120 (a) CS-ZnS/UV, (b) CS-ZnO /UV, (c) CS-ZnS/solar and (d) CS-ZnO/solar: [RR 120] = 50 ppm; catalyst suspended = 50 mg/100 mL; pH=5.

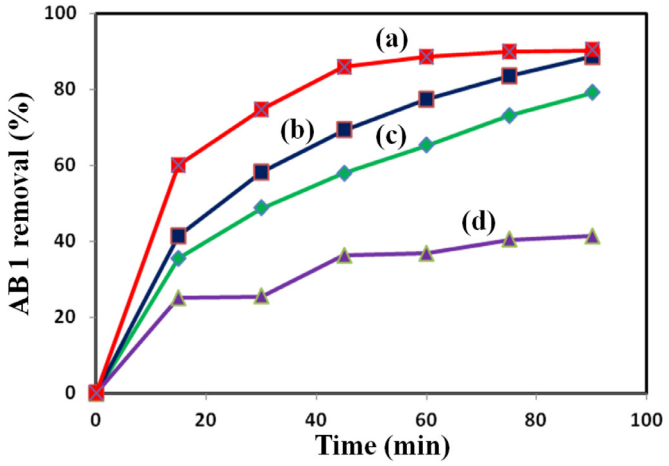

Fig. 11. Photodegradability of AB 1 dye (a) CS-ZnS (decolourization), (b) CS-ZnO (decolourization), (c) CS-ZnO (degradation), (d) CS-ZnS (degradation): [AB 1] = 10 ppm; catalyst suspended = 50 mg/100 mL; pH = 6.8.

decolourization increases from 58 to 82 and 87 to 96 when pH increases from 3 to 5 for CS-ZnO/UV and CS-ZnS/UV processes, respectively. After pH 5, there was a decrease in decolourization efficiency in both processes. The optimum pH for efficient removal of RR 120 dye is found to be 5 for both processes. The effect of pH on dye degradation and its important in the degradation process were reported earlier [27,28].

3.2.3. *Effect of catalyst loading*

Catalyst loading in slurry photocatalytic processes is an important factor that can strongly influence dye degradation. Experiments performed with different amounts of CS-ZnO and CS-ZnS under UV irradiation showed that the photodegradation efficiency increased with an increase in amount up to 50 mg/100 mL and then no significant change observed as shown in Fig. S4. The percentage of decolourization increases from 32 to 82 and 53 to 96 when catalyst increases from 10 mg/100 mL to 50 mg/100 mL for CS-ZnO/UV and CS-ZnS/UV processes, respectively. This observation

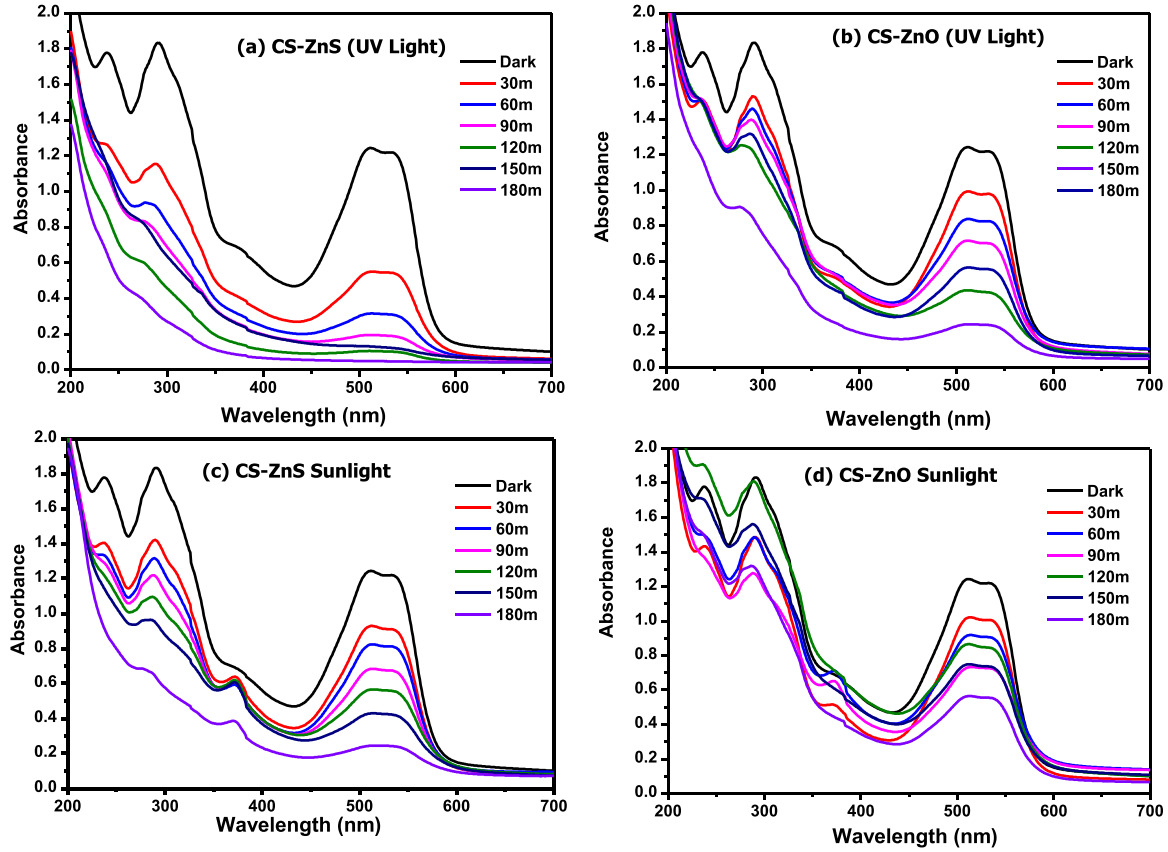

Fig. 10. UV–Visible spectra of the dye (RR 120) at different times of irradiation (a) CS-ZnS/UV, (b) CS-ZnO /UV, (c) CS-ZnS/solar and (d) CS-ZnO/solar: [RR 120] = 50 ppm; catalyst suspended = 50 mg/100 mL; pH=5.

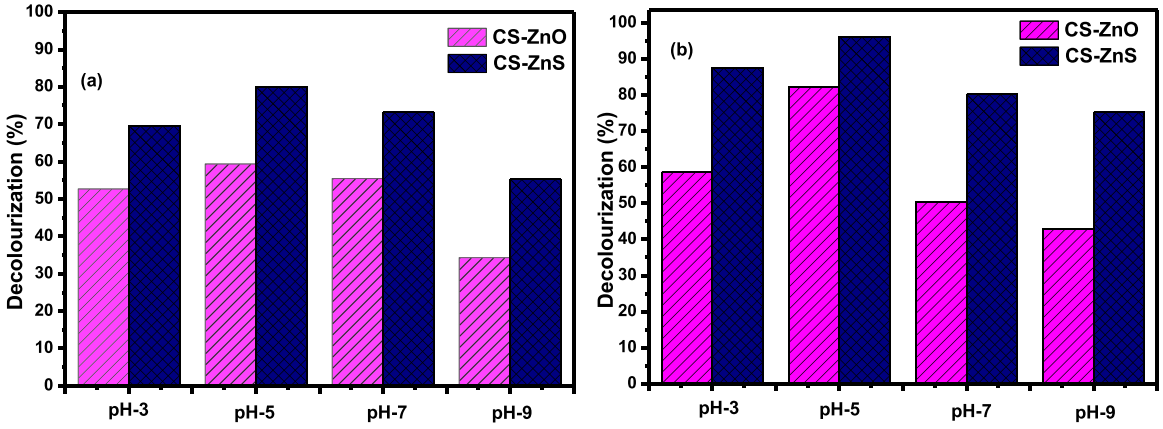

Fig. 12. Effect of pH on RR 120 decolourization by CS-ZnO and CS-ZnS (a) Sunlight and (b) UV light: [RR 120] = 50 ppm; catalyst suspended = 50 mg/100 mL.

Table 1
Mass spectral data of identified intermediates RR 120 by CS-ZnO.

S.No	Compounds	Retention Time (min)	m/e values
1	**D1** ($C_{12}H_{11}N_9$)	39.555	281.0 (M^+), 207.0, 191.0, 147.0, 135.0, 117.0, 105.0, 95.0, 77.0, 55.0
2	**D2** ($C_3H_4N_4$)	34.080	96.0 (M^+), 81.0, 69.0, 67.0, 55.0, 39.0, 29.0, 27.0
3	**D3** ($C_6H_6O_4$)	6.815	142.0 (M^+), 71.0, 57.0, 41.0, 29.0

can be explained in terms of availability of active sites on the catalyst surface and penetration [27-29].

3.3. Reusability

The application may be extended for pilot or industrial scale level, catalyst lifetime is an important parameter for these applications because its use for a longer time leads to a significant cost reduction of the treatment. For this reason, the catalysts were recycled, and the results are shown in Fig. S5. For CS-ZnO, about 82%, 80%, 77% and 64% of decolourization observed for 1st, 2nd, 3rd and 4th run, respectively. In the case of CS-ZnS, about 96%, 94%, 92%, and 77% of decolourization observed for 1st, 2nd, 3rd, and 4th run, respectively. There was no significant decrease in activity observed for CS-ZnO and CS-ZnS up to 3rd run, after that, there is a slight decrease in activity observed for both catalysts.

3.4. GC–MS analysis

An attempt has been made to identify the intermediate products formed during photodegradation of RR 120 by CS-ZnO and CS-ZnS under UV irradiation. It has been analyzed through GC–MS analysis, and suitable degradation pathways are proposed in Scheme 1 and Scheme 2, respectively. Sometimes, organic pollutant degradation may take place through the formation of harmful intermediates that are more toxic than the original compounds. Therefore, the knowledge on the identity of the intermediates is a necessity in these degradation processes. A degradation pathway of RR 120 by CS-ZnO was proposed based on m/e ratio, retention time, and its molecular weight from GC–MS analysis (Scheme 1). GC–MS analysis reveals that the three peaks with the retention time of 6.815, 34.080, and 39.555. Molecular ion and fragmentation peak values for these identified intermediates are given in Table 1. During the photocatalytic degradation process, it was observed that the cleavage of azo linkage takes place first before that sulfonyl groups of RR 120 being replaced by a hydroxyl group, leading to the formation of compounds (**I and II**) shown in the pathway (Scheme 1). It was thus assumed that the hydroxyl radicals were the major reactive species in this study. The intermediate compound **I** undergoes C–N cleavage and dechlorination produced intermediate product N^2-(4-(1,3,5-triazin-2-ylamino)phenyl)−1,3,5-triazine-2,4-diamine (**D1**) and compound **III**. The intermediate product **D1** further cleaved by the repetitive attack of •OH radicals produced intermediate 1,3,5-triazin-2-amine (**D2**) and compound **IV**. The repetitive attack of •OH radicals into intermediate compound III undergoes deamination and naphthalene ring cleavage produced benzene-1,2,3,5-tetraol (**D3**). The compound **II** undergoes deamination produced intermediate compound **V**. Finally, it is expected that the compounds **D2, D3**, compound **IV**, and compound **V** undergo further degradation to produced unidentified non toxic compounds, CO_2, water, and mineral acids [30-32].

The photodegradation of RR 120 was started by the initial cleavage of azo bonds (Scheme 2), produced two intermediates **I** and **II**. GC–MS analysis reveals that the two peaks with the retention time of 23.555 and 32.980. Molecular ion and fragmentation peak values for these identified intermediates are given in Table 2. The intermediate **I** undergoes dechlorination and ring cleavage produced 8-(4-(N-substituted)−1,3,5-triazin-2-ylamino)−2-aminonaphthalene derivative (**D1**) which on further degradation produced 2,8-diaminonaphthalene-1,3,6-triol (**D2**) and compound **III**. Compound **II** undergoes deamination produced compound **IV**. Finally, these by-products (**D2**, compound **III** and compound **IV**) would be mineralized to CO_2 and H_2O.

3.5. Mechanism of degradation

When CS-ZnO or CS-ZnS is irradiated by UV or solar light, the electrons are excited to the conduction band (CB), leaving holes in

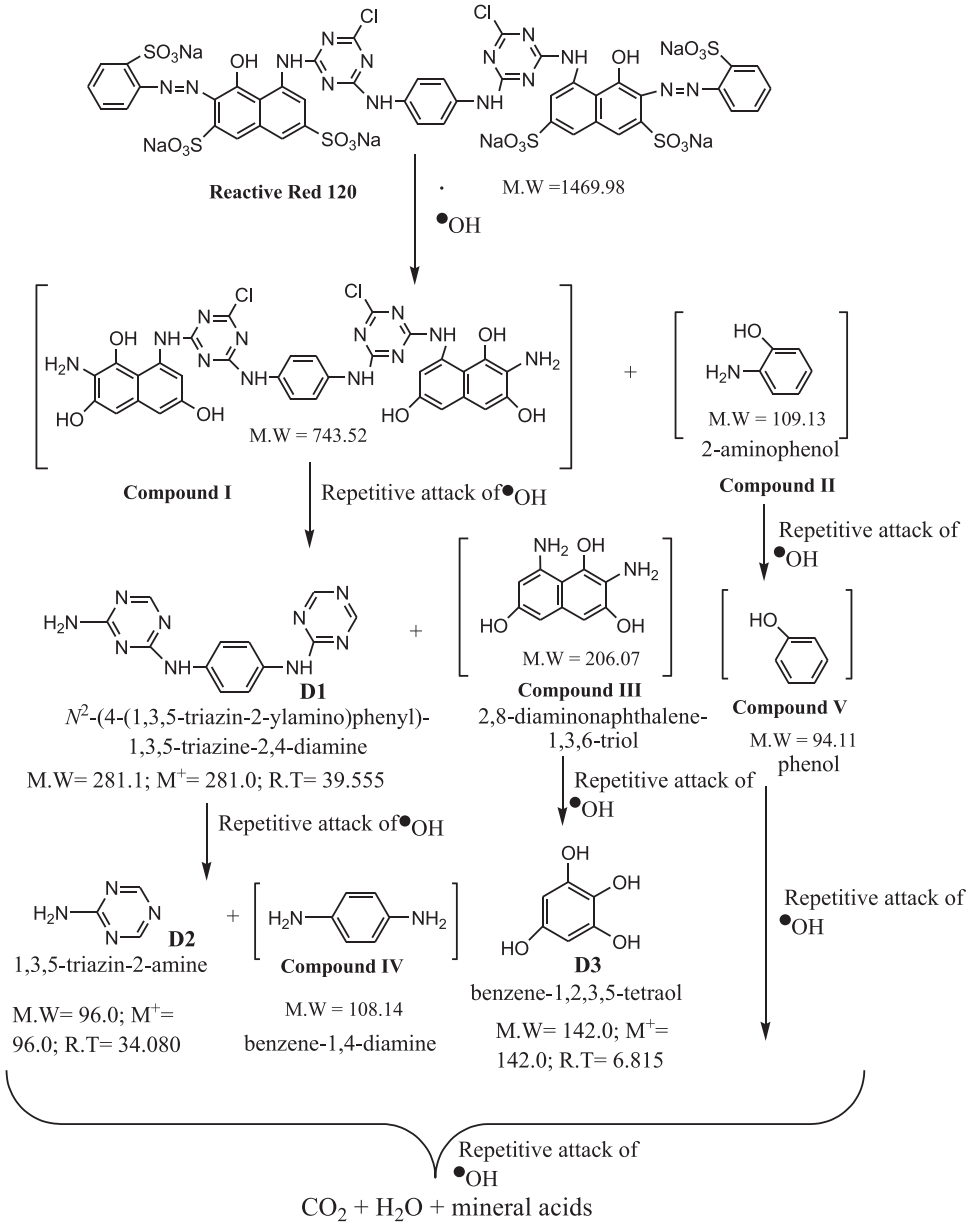

Scheme 1. Degradation pathway of RR 120 by CS-ZnO .

Table 2
Mass spectral data of identified intermediates RR 120 by CS-ZnS.

S.No	Compounds	Retention Time (min)	m/e values
1	**D1** ($C_{20}H_{20}N_{10}O_3$)	23.555	449.0 (M^+), 435.0, 429.0, 405.0, 363.0, 347.0, 313.0, 267.0, 239.0, 177.0, 163.0, 147.0, 133.0, 93.0, 73.0, 59.0, 45.0, 43.0
2	**D2** ($C_{10}H_{10}N_2O_3$)	32.980	207.0 (M + 1), 147.0, 129.0, 112.0, 83.0, 70.0, 57.0

the valence band (VB), and the as-formed electron–hole pairs are responsible for the photocatalytic activities of CS-ZnX ($X = O$ or S) (Scheme S1). The electrons in the conduction band react with O_2 to form superoxide anion radicals ($O_2^{\bullet-}$), the holes in the valence band react with water to form hydroxyl radicals ($^{\bullet}OH$). The superoxide radical anion and hydroxyl radical are mainly used for dye degradation [33-35].

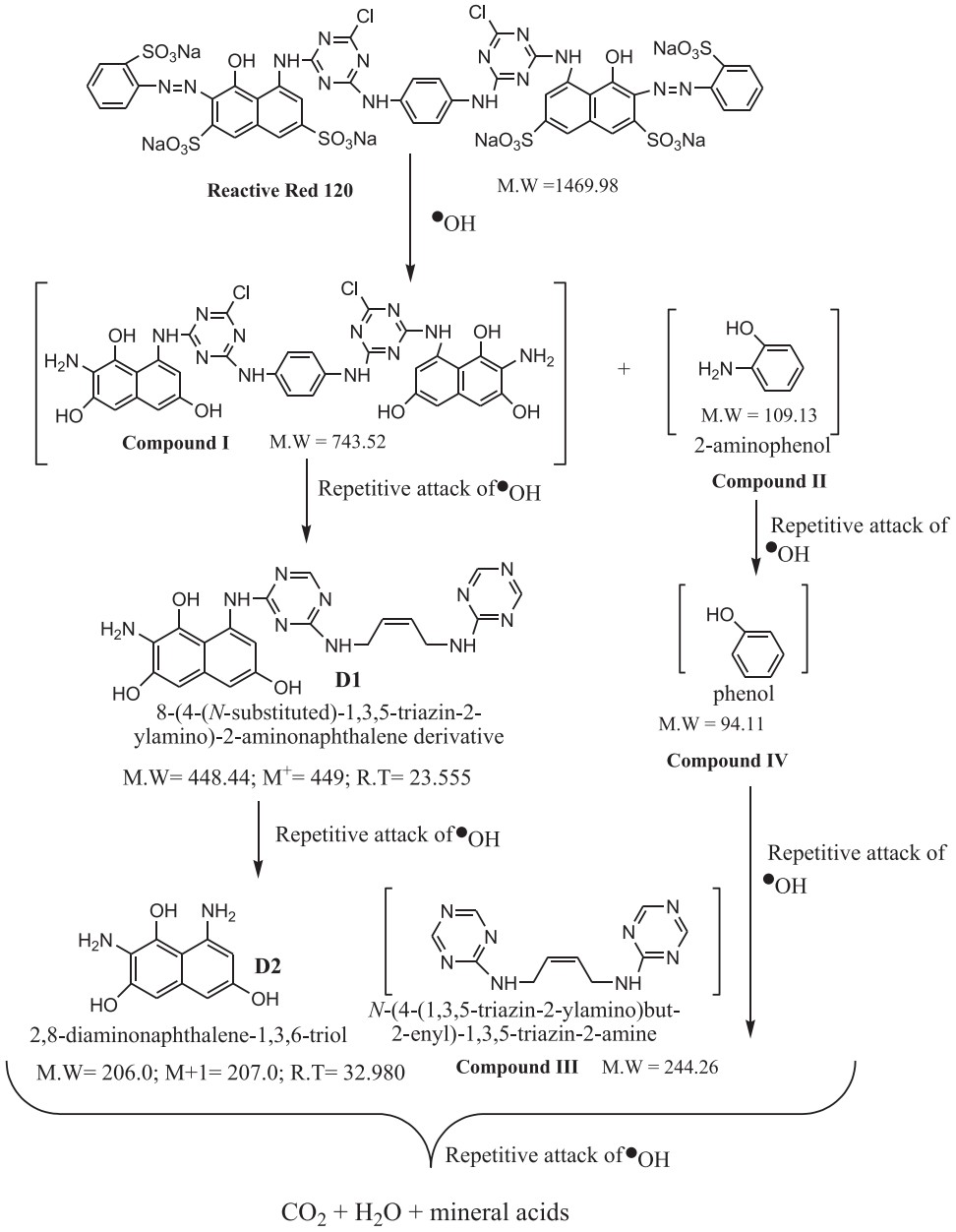

Scheme 2. Degradation pathway of RR 120 by CS-ZnS .

4. Conclusions

Costus speciosus Koen leaf extract assisted ZnX (*X* = *O* or S) nanomaterials were synthesized by precipitation cum hydrothermal method. The prepared materials were characterized by FT-IR, XRD, Raman, UV-DRS, FE-SEM, HR-TEM, EDS, and PL measurements. The photocatalytic activity of these catalysts has been tested in the degradation of RR 120 dye under UV and solar light. The activity of the materials was also tested toward AB 1 dye degradation. The optimum pH and catalyst loading for efficient removal of RR 120 dye are found to be 5 and 50 mg/100 mL, respectively. The order of activity for RR 120 dye decolourization is found to be CS-ZnS (UV) > CS-ZnO (UV) > CS-ZnS (solar) > CS-ZnO (solar). Degradation pathways were proposed for RR 120 dye degradation using GC–MS analysis, and GC–MS analysis reveals the formation of N^2-(4-(1,3,5-triazin-2-ylamino)phenyl)−1,3,5-triazine-2,4-diamine, 1,3,5-triazin-2-amine and benzene-1,2,3,5-tetraol as intermediates for CS-ZnO/RR 120/ UV process. In CS-ZnS/RR 120/UV process the intermediates are found to be 8-(4-(N-substituted)−1,3,5-triazin-2-ylamino)−2-aminonaphthalene derivative and 2,8-diaminonaphthalene-1,3,6-triol and also GC–MS analysis proves that mineralization of RR 120 dye with CS-ZnX (*X* = *O* or S) catalysts. A suitable degradation mechanism was proposed for dye degradation by CS-ZnX (*X* = *O* or S) catalysts. These results show that CS-ZnX (*X* = *O* or S) catalysts have a significant role in RR 120 and AB 1 dye degradations, and as such these materials applications could be extended to the development of a photocatalyst which is applicable in both environmental purification and energy production processes.

Author's statement

S. Ravikumar is involved in the preparation of the materials and specifically writing the initial draft. V. Pandiyan and Balu Krishnakumar both are equally contributed in the supervision and leadership responsibility for the research activity planning and execu-

tion, including mentorship external to the core team. Manawwer Alam and Naushad Ahmad are involved in materials characterization. V. Nithya and Abilio J. F. N. Sobral are involved in the validation of the manuscript and overall replication/ reproducibility of results/experiments and other research outputs.

Acknowledgments

Manawwer Alam is grateful to the Research Supporting Project number (RSP-2020/113), Saud University, Riyadh, Saudi Arabia for support. V.P is highly thankful to DST Science & Engineering Research Board (SERB through major research project grant F. No. EMR/2017/003583) and DST-FIST under grant F. No (SR/FST/College-2018–372 (c)) for providing financial assistance to carry out the research work. V.N is highly thankful to authorities of the Alagappa University, Karaikudi, Tamilnadu, India, which was supported the research work done by the MHRD-RUSA 2.0-F.24/51/2014-U, policy (TNMulti-Gen), Dept. of Edn. Govt. of India. One of the authors B.K is greatly acknowledged FCT postdoc-grant (SFRH/BPD/86971/2012) and Centro de Quimica (CQC) of University of Coimbra.

Supplementary materials

Supplementary material associated with this article can be found, in the online version, at doi:10.1016/j.molstruc.2020.129176.

References

[1] N. Birjandi, H. Younesi, N. Bahramifar, S. Ghafari, A.A. Zinatizadeh, S. Sethupathi, Optimization of coagulation-flocculation treatment on paper-recycling wastewater: application of response surface methodology, J. Environ. Sci. Health A. Tox. Subst. Environ. Eng. 48 (2013) 1573–1582.
[2] P. Sunghoon, A. Soyeon, K. Hyunsung, S. Lee, C. Lee, structure Synthesis, and UV-enhanced gas sensing properties of Au-functionalized ZnS nanowires, Sens. Actuators B: Chem. 188 (2013) 1270–1276.
[3] J.N. Hart, M. Cutini, N.L. Allan, Band gap modification of ZnO and ZnS through solid solution formation for applications in photocatalysis, Energy Procedia 60 (2014) 32–36.
[4] K.R. Raksha, S. Ananda, Study of kinetics of photocatalysis, bacterial inactivation and •OH scavenging activity of electrochemically synthesized Se^{4+} doped ZnS nanoparticles, J. Mol. Catal. A: Chem. 396 (2015) 319–327.
[5] M. Kaur, C.M. Nagaraja, Template-free synthesis of ZnS nanocrystals with a new sulfur source and their photocatalytic study, Mater. Lett. 154 (2015) 90–93.
[6] X. Fang, T. Zhai, U.K. Gautam, L. Li, L. Wu, Y. Bando, D. Golberg, ZnS nanostructures: from synthesis to applications, Prog. Mater. Sci. 56 (2011) 175–287.
[7] J.S. Jang, C.-J. Yu, S.H. Choi, S.M. Ji, E.S. Kim, J.S. Lee, Topotactic synthesis of mesoporous ZnS and ZnO nanoplates and their photocatalytic activity, J. Catal 254 (2008) 144–155.
[8] T.K. Tran, W. Park, W. Tong, et al., Photoluminescence properties of ZnS epilayers, J. Appl. Phys. 81 (1997) 2803–2809.
[9] H.C. Ong, R.P.H. Chang, Optical constants of wurtzite ZnS thin filmsdetermined by spectroscopic ellipsometry, Appl. Phys. Lett. 79 (2001) 3612–3614.
[10] W. Bai, X. Tian, R. Yao, Y. Chen, H. Lin, J. Zheng, Y. Xu, J. Lin, Preparation of nano-TiO_2@polyfluorene composite particles for the photocatalytic degradation of organic pollutants under sunlight, Sol.Energy. 196 (2020) 616–624.
[11] C. Liu, Y.A. Gorby, J.M. Zachara, J.K. Fredrickson, C.F. Brown, Reduction kinetics of Fe (III), Co (III), U (VI), Cr (VI), and Tc (VII) in cultures of dissimilatory metal-reducing bacteria, Biotechnol. Bioeng. 80 (2002) 637–649.
[12] P. Mukherjee, A. Ahmad, D. Mandal, S. Senapati, S.R. Sainkar, M.I. Khan, R. Ramani, R. Parischa, P. Ajayakumar, M. Alam, Angew, Bioreduction of $AuCl_4-$ Ions by the Fungus, Verticillium sp. and Surface Trapping of the Gold Nanoparticles Formed, Chem. Int. Ed. 40 (2001) 3585–3588.
[13] P. Yong, N.A. Rowson, J.P.G. Farr, I.R. Harris, L.E. Macaskie, Bioreduction and biocrystallization of palladium by Desulfovibrio desulfuricans NCIMB 8307, Biotechnol. Bioeng 80 (2002) 369–379.
[14] L. Lin, W. Wang, J. Huang, Q. Lia, D. Sun, X. Yang, H. Wang, N. He, Y. Wang, Nature factory of silver nanowires: plant-mediated synthesis using broth of Cassia fistula leaf, J. Chem. Eng. 162 (2010) 852–858.
[15] S.S. Shankar, A. Ahmad, R. Pasricha, M. Sastry, Bioreduction of chloroaurate ions by geranium leaves and its endophytic fungus yields gold nanoparticles of different shapes, J. Mater. Chem. 13 (2003) 1822–1826.
[16] X. Yang, Q. Li, H. Wang, J. Huang, L. Lin, W. Wang, D. Sun, Y. Su, J.B. Opiyo, L. Hong, Green synthesis of palladium nanoparticles using broth of Cinnamomum camphora leaf, J. Nanopart. Res. 12 (2010) 1589–1598.
[17] C. Surya, N. Agnel Arul John, V. Pandiyan, P. Amutha, Abílio J.F.N. Sobral, B. Krishnakumar, Antioxidant (*in vitro*), Antidiabetic (*in vitro*) and Photocatalytic Activity of *Costus speciosus* Leaf Extract Assisted CS-Ag-TiO_2 Composites, Toxicol. Environ. Health. Sci. 11 (2019) 197–209.
[18] C. Surya, N. Agnel Arul John, V. Pandiyan, S. Ravikumar, P. Amutha, Abilio J.F.N. Sobral, B. Krishnakumar, *Costus speciosus* Leaf Extract Assisted CS-Pt-TiO_2 Composites: synthesis, Characterization and their Bio and Photocatalytic Applications, J. Mol. Struct. 1195 (2019) 787–795.
[19] B. Krishnakumar, R. Hariharan, V. Pandiyan, Abilio J.F.N. Sobral, Gelatin-assisted g- TiO_2/BiOI heterostructure nanocomposites for azo dye degradation under visible light, J, Environ. Chemical Eng. 6 (2018) 4282–4288.
[20] Z.M. Khoshhesab, M. Sarfaraz, M.A. Asadabad, Preparation of ZnO nanostructures by chemical precipitation method, Synth. React. Inorg. Met.-Org. Chem. 41 (2011) 814–819.
[21] C.u Z.Mao, X.Chen X.Pan, W.Wang H.He, Z.Ye Y.Zeng, Raman-based measurement of carrier concentration in n-type ZnO thin films under resonant conditions, Phys. Lett.A. 384 (2020) 126148.
[22] B. Krishnakumar, T. Imae, J. Miras, J. Esquena, Synthesis and Azo Dye Photodegradation Activity of ZrS_2-ZnO Nanocomposites, Sep. Purif. Technol. 132 (2014) 281–288.
[23] Z. Ye, L. Kong, F. Chen, Z. Chen, Y. Lin, C. Liu, A comparative study of photocatalytic activity of ZnS photocatalyst for degradation of various dyes, Optik (Stuttg) 164 (2018) 345–354.
[24] L. Zhao, Y. Wang, A. Wang, X. Lia, C. Song, Y. Hu, Cr–doped ZnS semiconductor catalyst with high catalytic activity for hydrogen production from hydrogen sulfide in non- thermal plasma, Catal. Today 337 (2019) 83–89.
[25] B. Poornaprakash, D. Amaranatha Reddy, G. Murali, N. Madhusudhana Rao, R.P. Vijayalakshmi, B.K. Reddy, Composition dependent room temperature ferromagnetism and PL intensity of cobalt doped ZnS nanoparticles, J. Alloys Compd 577 (2013) 79–85.
[26] S.M. Mosavi, H. Kafashan, Physical properties of Cd-doped ZnS thin films, Superlattices Microstruct 126 (2019) 139–149.
[27] B. Subash, B. Krishnakumar, M. Swaminathan, M. Shanthi, Highly Efficient, Solar Active and Reusable Photocatalyst, Zr loaded Ag-ZnO for Reactive Red 120 Dye Degradation with Synergistic Effect and Dye Sensitized Mechanism, Langmuir 29 (2013) 939–949.
[28] B. Krishnakumar, T. Imae, Chemically Modified Novel PAMAM-ZnO Nanocomposite: synthesis, Characterization and Photocatalytic Activity, Appl. Catal. A 486 (2014) 170–175.
[29] A. Senthilraja, B. Subash, B. Krishnakumar, D. Rajamanickam, M. Swaminathan, M. Shanthi, Synthesis, Characterization and Catalytic Activity of co-doped Ag-Au-ZnO for MB Dye Degradation under UV-A Light, Mater. Sci. Semicond. Process 22 (2014) 83–91.
[30] B. Krishnakumar, B. Subash, M. Swaminathan, AgBr-ZnO – An Efficient Nano-photocatalyst for the Mineralization of Acid Black 1 with UV Light, Sep. Purif. Technol. 85 (2012) 35–44.
[31] R. Velmurugan, B. Krishnakumar, M. Swaminathan, Synthesis of Pd co-doped Nano-TiO_2-SO_4^{2-} and its Synergetic Effect on the Solar Photodegradation of Reactive Red 120 Dye, Mater. Sci. Semicond. Process 25 (2014) 163–172.
[32] A. Senthilraja, B. Krishnakumar, B. Subash, Abilio J.F.N. Sobral, M. Swaminathan, M. Shanthi, Sn loaded Au-ZnO Photocatalyst for the Degradation of AR 18 Dye under UV-A light, J. Ind. Eng. Chem. 33 (2016) 51–58.
[33] B. Subash, B. Krishnakumar, M. Swaminathan, M. Shanthi, ZnS-Ag-ZnO as an Excellent UV light Active Photocatalyst for the Degradation of AV 7, AB 1, RR 120 and RY 84 Dyes; Synthesis, Characterization and Catalytic Applications, Ind. Eng. Chem. Res. 53 (2014) 12953–12963.
[34] P. Dhatshanamurthi, B. Subash, B. Krishnakumar, M. Shanthi, Highly active ZnS loaded TiO_2 Photocatalyst for Mineralization of Phenol Red Sodium Salt under UV-A Light, Indian J. Chem. 53A (2014) 820–823.
[35] B. Krishnakumar, M. Swaminathan, Solar Photocatalytic Degradation of Acid Black 1 with ZnO, Indian J. Chem. 49A (2010) 1035–1040.